ENCYCLOPEDIA OF EARTH SCIENCES SERIES

ENCYCLOPEDIA *of* PLANETARY SCIENCES

edited by

JAMES H. SHIRLEY *and*
RHODES W. FAIRBRIDGE

CHAPMAN & HALL

London · Weinheim · New York · Tokyo · Melbourne · Madras

Published by Chapman & Hall, 2–6 Boundary Row, London SE1 8HN, UK

Chapman & Hall, 2–6 Boundary Row, London SE1 8HN, UK

Chapman & Hall GmbH, Pappelallee 3, 69469 Weinheim, Germany

Chapman & Hall USA, 115 Fifth Avenue, New York, NY 10003, USA

Chapman & Hall Japan, ITP-Japan, Kyowa Building, 3F,
2–2–1 Hirakawacho, Chiyoda-ku, Tokyo 102, Japan

Chapman & Hall Australia, 102 Dodds Street, South Melbourne,
Victoria 3205, Australia

Chapman & Hall India, R. Seshadri, 32 Second.Main Road, CIT East,
Madras 600 035, India

First edition 1997

Typeset in 8/8½pt Times by Photoprint, Torquay, Devon

Printed and bound in Croatia by Zrinski d.d., Cakovec

ISBN 0 412 06951 2

A catalogue record for this book is available from the British Library

Library of Congress Catalog Card Number: 96–86590

wind, solar wind plasma enters the magnetosphere, becoming the primary source of plasma in the case of Mercury's small magnetosphere and secondary plasma sources at Earth, Uranus and Neptune. In the magnetospheres where plasma flows are dominated by the planet's rotation (Jupiter, Saturn and within the Earth's plasmasphere), the plasma is confined by the planet's strong magnetic field for many days so that substantial densities are accumulated.

Thus we can identify three categories of planetary magnetospheres:

1. the large, symmetric and rotation-dominated magnetospheres of Jupiter and Saturn;
2. the small magnetosphere of Mercury where the only source of plasma is the solar wind which drives rapid circulation of material through the magnetosphere; and
3. the moderate-sized and highly asymmetric magnetospheres of Uranus and Neptune, whose constantly changing configuration does not allow substantial densities of plasma to build up. The Earth's magnetosphere is an interesting hybrid of the first two types, with a dense corotating plasmasphere close to the planet and tenuous plasma, circulated by the solar wind driven convection, in the outer region (Bagenal, 1992; Russell, Baker and Slavin, 1988; Parks, 1990).

Fran Bagenal

Bibliography

Acuna, M.H., Ness, N.F. (1976) The main magnetic field of Jupiter. *J. Geophys. Res.*, **81**, 2917–22.

Bagenal, F. (1992) Giant planet magnetospheres. *Ann. Rev. Earth Planet. Sci.*, **20**, 289.

Bagenal, F., Belcher, J.W., Sittler, E.C. and Lepping, R.P. (1987) The Uranian bow shock: Voyager 2 inbound observations of a high Mach number shock. *J. Geophys. Res.*, **92**, 8603–12.

Bame, S.J., Martin, R.H., Comas D.J. *et al.* (1989) Three-dimensional plasma measurements from three-axis stabilized spacecraft, in *Solar System Plasma Physics* (eds J.H. Waite, J.L. Burch and R.L. Moore). American Geophysical Union Publications.

Belcher, J.W. (1987) The Jupiter–Io connection: an Alfven engine in space, *Science*, **238**, 170.

Biermann, L. (1957) Solar corpuscular radiation and the interplanetary gas. *Observatory*, **77**, 109.

Cheng, A.F., Johnson, R.E. (1989) Effects of magnetosphere interactions on origin and evolution of atmospheres, in *Origin and Evolution of Planetary and Satellite Atmospheres* (eds S.K. Atreya, J.B. Pollack and M.S. Matthews) Tucson: University of Arizona Press.

Chapman, S. and Ferraro, V.C.A. 1931. A new theory of magnetic storms. *Terr. Magn. Atmos. Elect.*, **36**, 77–97.

Connerney, J.E.P. (1987) The magnetospheres of Jupiter, Saturn, and Uranus. *J. Geophys. Res.*, **25**, 615–38.

Connerney, J.E.P., Acuña, M.H. and Ness, N.F. (1991) The magnetic field of Neptune. *J. Geophys. Res.*, **96**, 19023.

Dessler, A.J. (ed.) (1983) *Physics of the Jovian Magnetosphere*. Cambridge University Press.

Gold, T. (1959) *Symposium on the Exploration of Space* **64**, pp. 1665–1674

Hill, T.W. and Dessler, A.J. (1991) Plasma motions in planetary magnetospheres. *Science*, **252**, 410–415.

Luhmann, J.G. (1986) The solar wind interaction with Venus. *Space Sci. Rev.*, **44**, 241.

Luhmann, J.G., Russell, C.T., Brace L.H. and Vaisberg, O.L. (1992) The intrinsic magnetic field and solar wind interaction of Mars, in *Mars* (eds H.H. Kieffer, B.M. Jakosky, C.W. Snyder and M.S. Matthews). Tucson: University of Arizona Press.

Marsch, E. and Schwenn, R. (eds) (1992) *Solar Wind Seven*. Pergamon Press.

Mendillo, M., Baumgardner, J., Flynn, B. and Hughes, J. (1990) The extended sodium nebula of Jupiter. *Nature*, **348**, 312–4

Moses, S.L., Coroniti, F.V., Kennel, C.F. *et al.* (1990). Comparison of plasma wave measurements in the bow shocks at Earth, Jupiter, Saturn, Uranus, and Neptune. *Geophys. Res. Lett.*, **17**, 1653–6.

Neubauer, F.M., Luttgen, A. and Ness, N.F. (1991). On the lack of a magnetic signature of Triton's magnetospheric interaction on the Voyager 2 flyby trajectory. *J. Geophys. Res.*, **96**, 19171–5.

Pizzo, V.J., Holzer, T. and Sime, D.G. (eds) (1988) *Proc. Sixth Int. Solar Wind Conf.*, High Altitude Observatory, NCAR, Boulder.

Parks, G.K. (1991) *Physics of Space Plasmas*. Addison-Wesley.

Priest, E. (ed)(1985) *Solar System Magnetic Fields*, Dordrecht: D. Reidel, pp. 224–56.

Russell, C.T. Hoppe, M.M. and Livesey, W.A. (1982). Overshoots in planetary bow shocks. *Nature*, **296**, 45–8.

Russell, C.T., Baker D.N. and Slavin, J.A. (1988). The magnetosphere of Mercury, in *Mercury* (eds F. Vilas, C.R. Chapman and M.S. Mathews) Tucson: University of Arizona Press.

Siscoe, G.L. (1979). Towards a comparative view of planetary magnetospheres, in *Solar System Plasma Physics*, Vol II (eds C.F. Kennel, L.J. Lanzerotti and E.N. Parker). Amsterdam: North Holland, 402 pp.

Slavin, J.A., Smith, E.J., Spreiter, J.R. and Starhara, S.S. (1985) solar wind flow about the outer planets: gas dynamic modeling of the Jupiter and Saturn bow shocks. *J. Geophys. Res.*, **90**, 6275–86.

Van Allen, J.A. (1990) Magnetospheres, cosmic rays and the interplanetary medium, in *The New Solar System* (eds J.K. Beatty and A. Chaikin). Sky Publishing.

Young, D.T. (1989). Space plasma mass spectroscopy below 60 KeV, in *Solar System Plasma Physics* (eds J.H. Waite, J.L. Burch and R.L. Moore). American Geophysical Union Publications, pp. 143–58.

Young, D.T., Marshall J.A., Burch, J.L. *et al.* (1989). A 360° field of view toroidal ion composition analyzer using time of flight, in *Solar System Plasma Physics* (eds J.H. Waite, J.L. Burch and R.L. Moore). American Geophysical Union Publications, pp. 171–80.

Cross references

Alfvén wave
Aurora
Comet: dynamics
Ion and neutral mass spectrometry
Ionosphere
Magnetospheres of the outer planets
Planetary torus
Plasma wave
Radiation belt
Solar corona
Solar wind
Thermal plasma instrumentation

PLASMA WAVE

A plasma is an electrically neutral mixture of electrons and ions in which the kinetic energy greatly exceeds the interaction energy between the particles. Plasmas are produced (1) by collisions whenever a gas is heated to over a few thousand degrees, and (2) by photoionization, for example by ultraviolet radiation from the Sun. Plasmas are destroyed by recombination. Because of the very low densities that exist in interplanetary space and the correspondingly low recombination rates, almost all of the material that exists between the Sun and the planets is a plasma. This includes the solar corona, which is the hot ionized outer atmosphere of the Sun; the solar wind, which is an ionized gas streaming outward from the Sun at supersonic speeds; planetary magnetospheres, which are hot energetic plasmas surrounding planets with strong magnetic fields; and planetary ionospheres, which are layers of ionized gas in the upper regions of planetary atmospheres.

As in any fluid, waves can propagate through a plasma. Because of the electrical character of the plasma medium, plasma waves are very complex. Some of these waves have electric and magnetic fields, and are similar to the electromagnetic waves in free space. These are called electromagnetic waves. Others are more like sound waves and have no magnetic field. These are called electrostatic waves, since the electric field can be derived from the gradient of an electrostatic potential ($\vec{E} = -\vec{\nabla}\,\phi$). Usually, electromagnetic waves have propagation speeds near the speed of light, whereas electrostatic waves have propagation speeds near the speed of sound.

In most space plasmas the collision frequencies are very low. This type of plasma, with essentially zero collision frequency and infinite

Table P10 The most common plasma wave modes

Plasma wave mode	Frequency range	Electromagnetic/ electrostatic	Polarization	Free energy source
Free-spaced (L,O) mode	$\omega > \omega_{pe}$	Electromagnetic	L	Beam, loss cone
Free-space (R,X) mode	$\omega > \omega_{R=0}$	Electromagnetic	R	Beam, loss cone
Electron plasma oscillations (Langmuir waves)	$\omega \simeq \omega_{pe}$	Electrostatic	–	Beam
Z mode	$\omega_{UHR} > \omega > \omega_{L=0}$	Electromagnetic, electrostatic near ω_{UHR}	R for $\omega > \omega_{pe}$ L for $\omega > \omega_{pe}$	Beam
Electron cyclotron waves	Bands near $\omega \simeq (n + \frac{1}{2})\omega_{ce}$	Electrostatic	–	Ring distribution (electrons)
Whistler mode	$\omega < \text{Min}\ \{\omega_{ce}, \omega_{pe}\}$	Electromagnetic, electrostatic near ω_{LHR}	R	Loss cone, beam above ω_{LHR}
Ion-acoustic mode	$\omega \lesssim \omega_{pi}$	Electrostatic	–	Drift between electrons and ions
Electrostatic ion cyclotron waves	Bands near $\omega \simeq (n + \frac{1}{2})\omega_{ci}$	Electrostatic	–	Ring distribution (ions) field-aligned currents
Electromagnetic ion cyclotron waves	$\omega << \omega_{ci}$	Electromagnetic	L	Pressure anisotropies

$\omega_{R=0} = \omega_{ce}/2 + ((\omega_{ce}/2)^2 + \omega_{pe})^{1/2}$
$\omega_{UHR} = (\omega_{ce}^2 + \omega_{pe}^2)^{1/2}$
$\omega_{L=0} = -\omega_{ce}/2 + ((\omega_{ce}/2)^2 + \omega_{pe}^2)^{1/2}$
$\omega_{LHR} \simeq (\omega_{ce}\,\omega_{ci})^{1/2}$ if $\omega_{pe} \gg \omega_{ce}$

mean free path, is called a collisionless plasma. The absence of collisions effectively eliminates the basic mechanism of energy and momentum exchange that normally exists between particles in a fluid. Under this circumstance, waves provide the primary mechanism for energy and momentum exchange. Waves then play a role somewhat similar to collisions in an ordinary gas. Whenever a sufficiently large deviation from thermal equilibrium occurs, waves grow spontaneously in the plasma. The non-equilibrium feature that gives rise to the wave growth is called a free energy source. Examples of free energy sources are beams and anisotropies in the velocity distribution of the particles. Once generated, the waves are eventually reabsorbed via a process known as collisionless damping. The wave growth and damping lead to an energy and momentum exchange. From very general principles it can be shown that the energy and momentum exchange acts to drive the plasma toward thermal equilibrium, very similar to collisions in an ordinary fluid. Waves therefore play a crucial role in maintaining the equilibrium state of the plasma.

Many different plasma wave modes exist in a plasma, particularly if the plasma has a magnetic field. These wave modes are usually associated with certain characteristic frequencies. The two primary characteristic frequencies of a plasma are the plasma frequency ω_p and the cyclotron frequency ω_c. A plasma frequency and a cyclotron frequency can be defined for each species present in the plasma. The electron plasma frequency is given by

$$\omega_{pe} = \left(\frac{e^2 n_e}{\epsilon_0 m_e} \right)^{1/2} \tag{P9}$$

where e is the electronic charge, n_e is the electron number density, ϵ_0 is the permittivity of free space and m_e is the electron mass. The electron plasma frequency is the characteristic oscillation frequency that occurs whenever electrons are perturbed from their equilibrium position in the plasma. The electron cyclotron frequency is given by

$$\omega_{ce} = \frac{eB}{m_e} \tag{P10}$$

where B is the magnetic field. The electron cyclotron frequency is the characteristic rotation frequency that occurs whenever an electron has a component of velocity perpendicular to the magnetic field. Comparable equations for the ion plasma frequency and ion cyclotron frequency are obtained by changing (e) to (i) in equations (P9) and (P10). In addition to the electron and ion plasma frequencies and cyclotron frequencies, it is convenient to define four additional characteristic frequencies. These are: the upper hybrid resonance frequency,

$$\omega_{UHR} = (\omega_{pe}^2 + \omega_{ce}^2)^{1/2} \tag{P11}$$

the lower hybrid resonance frequency,

$$\omega_{LHR} = (\omega_{ce}\,\omega_{ci})^{1/2} \tag{P12}$$

the right-hand cut-off,

$$\omega_{R=0} = \omega_{ce}/2 + ((\omega_{ce}/2)^2 + \omega_{pe}^2)^{1/2} \tag{P13}$$

and the left-hand cut-off.

$$\omega_{L=0} = -\omega_{ce}/2 + ((\omega_{ce}/2)^2 + \omega_{pe}^2)^{1/2} \tag{P14}$$

The relationships that these characteristic frequencies have to the various wave modes that exist in a plasma are summarized in Table P10. This table lists the commonly accepted name of the mode, the frequency range over which the mode can propagate, the electromagnetic/electrostatic character of the mode, the polarization (R,L) with respect to the magnetic field (when applicable) and the free energy source that can cause wave growth. It should be noted that Table P10 only applies to a plasma consisting of electrons and one positive ion species. If more than one positive ion species is present, then additional modes appear between adjacent pairs of ion cyclotron frequencies. For a further detailed discussion of the wave modes that can exist in a plasma, see Stix (1962) or Krall and Trivelpiece (1973).

Instrumentation

Space plasma wave measurements have been carried out by spacecraft-borne instrumentation for over 30 years. The first instruments specifically designed to study naturally occurring space plasma waves were launched on the Earth-orbiting Alouette 1 and Injun III satellites in 1962 (Barrington and Belrose, 1963; Gurnett and O'Brien, 1964). Since then many different types of plasma wave instruments have flown on Earth-orbiting and interplanetary spacecraft. These instruments usually have several characteristics in common. In order to distinguish between electromagnetic waves and electrostatic waves, both electric and magnetic fields must be measured. (The absence of a wave magnetic field indicates the wave is electrostatic.) Electric fields are usually detected by an electric dipole antenna that extends in opposite directions from the center of the spacecraft, as illustrated in Figure P28. The quantity measured is the voltage difference, $\Delta V = V_2 - V_1$, between the two antenna elements. The electric field component along the axis of the antenna is then given by $E = \Delta V/l_{eff}$, where l_{eff} is a quantity called the effective length. For wavelengths λ longer than the tip-to-tip length L of the antenna, the effective length is given by $l_{eff} = L/2$. A wide range of electric antenna lengths can be used, ranging from a fraction of a meter to over 200 m. Because the measured voltage ΔV increases with the antenna length, longer antennas are generally preferred since they give better sensitivity. A variety of mechanisms are used to extend the antenna. One technique uses centrifugal force to pull a fine wire

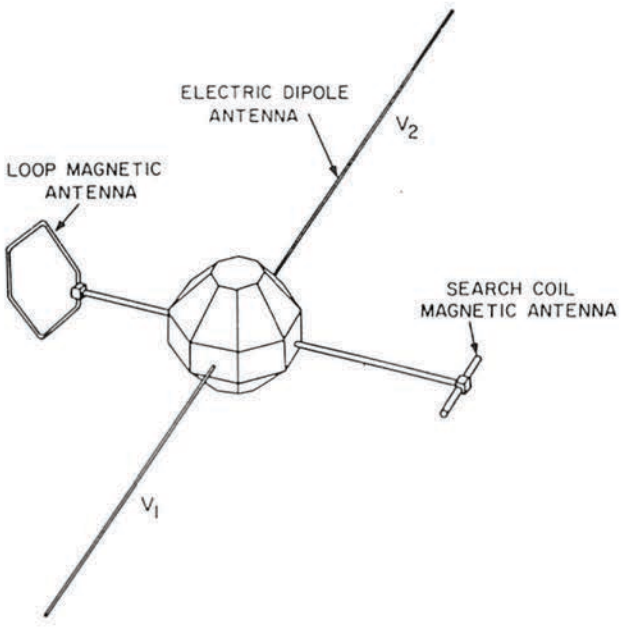

Figure P28 A typical antenna geometry for detecting space plasma waves. Electric fields are usually detected by an electric dipole antenna, and magnetic fields are detected by either a loop antenna or a search coil magnetometer.

radially outward from a fishing-reel type of dispenser in the spacecraft. This technique only works on spinning spacecraft. Another technique uses a motor-driven device to extrude a thin metal tape through a guide to form a rigid metal tube. This type of antenna works equally well on both spinning and non-spinning spacecraft. Sometimes small metal spheres with internal high impedance amplifiers are placed on the ends of the antenna to sense the potential in the plasma (Fahleson, 1967). In this case, the effective length is the center-to-center distance between the spheres.

Wave magnetic fields are usually detected using the magnetic induction principle, wherein a voltage is induced in a coil of wire by a time-varying magnetic field. The voltage induced is given by $V = N\mathrm{d}\Phi/\mathrm{d}t$, where $\Phi = AB$ is the magnetic flux through the coil, N is the number of turns, A is the cross-sectional area and B is the magnetic field strength. Two types of magnetic sensors are used. The first type is a loop antenna. Usually a loop antenna consists of a single turn, which minimizes the inductance and gives the maximum bandwidth. A transformer is usually used to couple the antenna to the electronics. The second type is a search coil magnetometer, which consists of a high-permeability rod surrounded by a sensing coil. The high-permeability rod acts to concentrate the magnetic flux through the coil, thereby increasing the sensitivity. Generally, loop antennas provide better sensitivities at higher frequencies, particularly above a few tens of kilohertz, whereas search coils provide better sensitivities at lower frequencies, below a few hundred hertz. To reduce interference from electrical systems on the spacecraft, magnetic field antennas must be mounted on booms away from the spacecraft body, as illustrated in Figure P28. In some cases multiple axis antennas are also used. Full three-axis measurements give information on the direction of propagation of a wave

The signals from the electric and magnetic antennas can be processed in a variety of ways. A typical block diagram of a plasma wave instrument is shown in Figure P29. Usually the antennas are connected to preamplifiers located close to the antennas. The preamplifiers are designed to provide low noise levels and to optimize the transmission of signals from the antennas to the main electronics package. The frequency range over which the antenna/preamplifier system must operate extends from the lowest characteristic frequencies of interest (usually f_{ci}) to the highest frequencies of interest (f_{pe} or f_{ce}). For planetary plasma wave investigations, this frequency range typically extends from a few hertz to a few megahertz.

Two different techniques are employed to process signals from electric and magnetic field sensors. In the first technique an onboard spectrum analyzer is used to generate spectrum amplitudes at a series of frequencies, $f_1, f_2, \ldots, f_n$. A spectrum analyzer of this type is shown in the top portion of the block diagram in Figure P29. The purpose of the onboard spectrum analysis is to provide continuous low-resolution survey spectrums using relatively modest telemetry rates, typically a few hundred bits per second. In the second technique a wideband receiver is used to transmit electric or magnetic field waveforms directly to the ground. The onboard signal processing is minimal, and the spectrum processing (Fourier analysis) is performed by ground-based computers. A wideband receiver is shown at the bottom of the block diagram in Figure P29. The main purpose of the wideband receiver is to limit the bandwidth of the signal and to control the amplitude of the signal by means of an automatic gain control. The waveform transmission can be either analog or digital. The advantage of the waveform measurements is the very high resolution. Since the entire waveform is transmitted, the resolution in frequency and time is limited only by the uncertainty principle ($\Delta\omega\Delta t \approx 1$). The disadvantage is that the telemetry rates are extremely high, often several hundred kbits per second or more. For this reason, wideband waveform transmissions are often of limited duration (60 s or less), thereby restricting the waveform measurements to a few specific samples, rather than continuous coverage. In this respect the onboard spectrum analysis and the wideband technique are complementary. The spectrum analyzer provides continuous low-resolution survey measurements, and the wideband receiver provides high-resolution spectrums for selected time intervals.

Observations

Spacecraft plasma wave observations have now been obtained at seven planets (Venus, Earth, Mars, Jupiter, Saturn, Uranus and Neptune). The most extensive measurements have been performed in the vicinity of Earth. Since the first such measurements in 1962 many spacecraft have provided plasma wave measurements in Earth orbit. These spacecraft have explored most of the near-Earth environment, with trajectories ranging from low-altitude orbits near the Earth, to highly eccentric orbits extending well beyond the orbit of the Moon. Plasma wave observations at the other planets are much more limited, and it is these measurements that will be emphasized here, since they are at the frontier of present day research. Of the various spacecraft that have flown to the other planets, the Voyager 1 and 2 mission to the giant planets, Jupiter, Saturn, Uranus and Neptune, has probably contributed the most to our expanding knowledge of space plasma waves. The giant planets, like the Earth, have strong magnetic fields and intense radiation belts, which make them a rich source of plasma waves. For the initial Voyager reports of plasma wave observations at the giant planets, see Scarf, Gurnett and Kurth (1979), Scarf *et al.* (1982), Gurnett, Kurth and Scarf (1979a, 1981) and Gurnett *et al.* (1986, 1989). The only other spacecraft that has provided plasma wave measurements at the giant planets is Ulysses, which flew by Jupiter in 1992. For the initial report of the Ulysses plasma wave observations, see Stone *et al.* (1992). The remaining two planets, Venus and Mars, have negligible internal magnetic fields and therefore fewer types of plasma wave phenomena. The first measurements of plasma waves in the vicinity of Venus were provided by the Pioneer Venus spacecraft, which was placed in orbit around Venus on 4 December 1979. The first report on the Pioneer Venus plasma wave observations was given by Scarf, Taylor and Green (1979). The only other spacecraft that has provided plasma wave observations in the vicinity of Venus is Galileo, which flew by Venus on 10 February 1990. For a report on the Galileo Venus plasma wave observations, see Gurnett *et al.* (1991). At Mars the first, and only, plasma wave measurements were obtained by the Phobos 2 spacecraft, which was placed in orbit around Mars on 29 January 1989. An initial report on the Phobos 2 plasma wave observations is given by Grard *et al.* (1991).

Since there are so many planets to review, no attempt will be made to describe the observations in detail at each planet. Instead, the observations will be organized according to the various types of plasma waves observed, ordered according to decreasing distance from the planet, starting from the Sunward side of the planet, and ending in the region near the closest approach. No discussion is given of electromagnetic radiation that can escape to great distances from the planet, since these waves are usually regarded as radio astronomi-

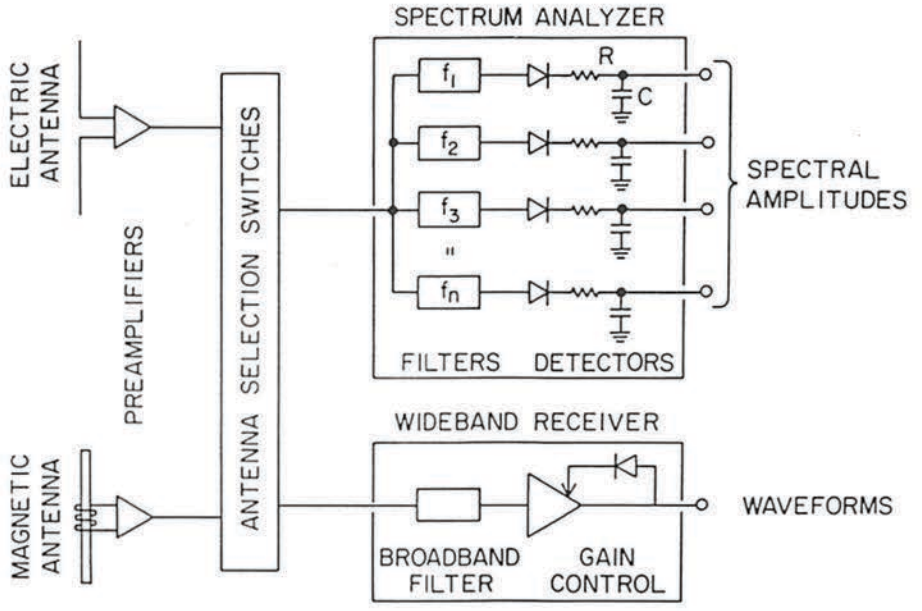

Figure P29 A block diagram of a typical plasma wave instrument. These instruments often consist of an onboard spectrum analyzer which gives low-resolution continuous spectrums, and a wideband waveform receiver which gives very high-resolution spectrums for selected intervals.

cal emissions. For a review of planetary radio emissions see Gurnett (1992).

Electron plasma oscillations and ion acoustic waves

The solar wind flows outward from the Sun at a nearly constant speed of about 400 km s^{-1}. At this speed the solar wind flow is supersonic. When the solar wind encounters a large object such as a planet, a shock wave is formed, very similar to the shock wave that forms upstream of an airplane in supersonic flight. This shock is called the bow shock. The approximate shape of the shock is shown in Figure P30. If the planet has no internal magnetic field, as in the case of Venus and Mars, the planet and its surrounding atmosphere and ionosphere act as the obstacle. The radial distance to the nose of the shock is then only slightly larger than the radius of the planet. If the planet has a strong internal magnetic field, as in the case of the Earth and the giant planets, the magnetic field acts as the obstacle. The position of the shock is then controlled by the strength of the planetary magnetic field. The interface between the solar wind and the planetary magnetic field is called the magnetopause (Figure P30). At Jupiter, for example, the nose of the shock is typically at 80 to 120 R_J (where R_J is the radius of the planet), and the magnetopause is at 50 to 70 R_J.

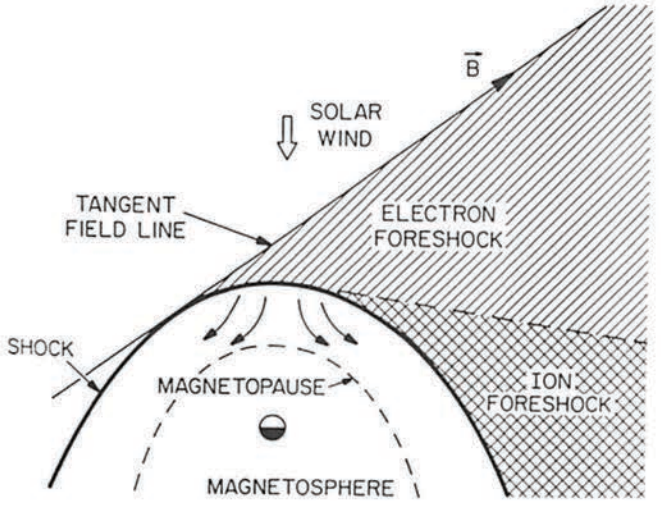

Figure P30 A sketch of the various boundaries and regions that occur in the solar wind upstream of a planet. Since the solar wind is supersonic, a shock wave forms upstream of the planet. Electrons and ions energized at the shock escape upstream into regions known as the electron foreshock and the ion foreshock.

At the shock the plasma is strongly heated and some of the electrons and ions escape upstream into the solar wind. Because the escaping particles are guided along the magnetic field lines by magnetic forces, these particles are confined to a region upstream of the shock called the foreshock. Usually the escaping electrons have very high speeds, typically 10^4 to 10^5 km s^{-1}, which is much greater than the solar wind speed. At these very high velocities, the region accessible to the backstreaming electrons is essentially delineated by the magnetic field lines tangent to the shock (Figure P30). This region is called the electron foreshock. The escaping ions, because of their higher mass, have much lower velocities, more nearly comparable to the solar wind speed. The region accessible to the backstreaming ions is therefore angled backward substantially from the tangent field line (Figure P30). This region is called the ion foreshock.

Because the backstreaming electrons constitute a beam, these particles can excite electron plasma oscillations, also sometimes called Langmuir waves (Table P9). Electron plasma oscillations excited by electrons streaming into the solar wind were first discovered by Scarf *et al.* (1971) upstream of the Earth's bow shock. Since then similar electron plasma oscillations have been discovered at Venus and Mars and at all four of the giant planets. A multichannel plot illustrating the occurrence of electron plasma oscillations upstream of Jupiter's bow shock is shown in Figure P31. These data are from the low-rate spectrum analyzer onboard Voyager 1. The enhanced emissions in the 5.62-kHz channel from about 12 : 18 to 12 : 27 UT are electron plasma oscillations. The electron plasma frequency f_{pe} during this interval was about 5.5 to 6.0 kHz. The onset of the plasma oscillations at 12 : 18 UT corresponds to the crossing of the tangent field line, and the termination at 12 : 27 UT corresponds to the crossing of the bow shock.

The frequency of upstream electron plasma oscillations generally decreases with increasing distance from the Sun. As can be seen from equation (P9), the electron plasma frequency is proportional to the square root of the electron density. Since the solar wind density varies roughly as $1/R^2$, where R is the distance from the Sun, the

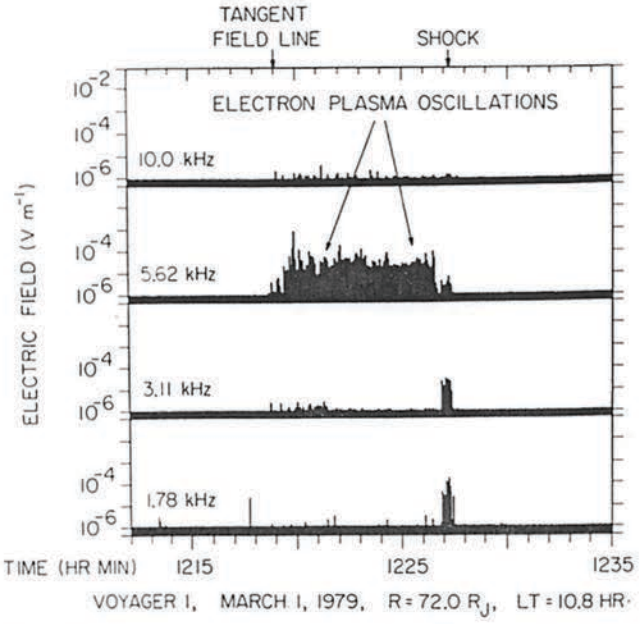

Figure P31 An example of electron plasma oscillations in the solar wind upstream of Jupiter. These waves occur in the electron foreshock and are produced by energetic (~ 1 to 10 keV) electron beams escaping into the solar wind from the bow shock.

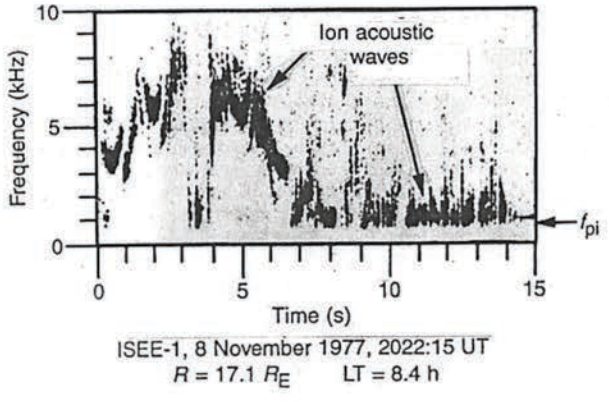

Figure P32 A high-resolution frequency–time spectrogram of ion acoustic waves observed in the solar wind upstream of the Earth's magnetosphere. These waves are produced by energetic (~ 10 keV) ions escaping into the solar wind from the bow shock.

electron plasma frequency varies roughly as $1/R$. At Venus the electron plasma frequency is typically about 30 kHz, whereas at Neptune the electron plasma frequency is about 700 Hz. The electric field strength of the plasma oscillations also decreases with increasing distance from the Sun. At Venus and Earth the peak field strengths are about 1 mV m^{-1}, whereas at Neptune the peak field strengths are about 30 to 100 μV m^{-1}.

In addition to electron plasma oscillations, another type of wave also occurs upstream of planetary bow shocks. These waves were first detected upstream of the Earth's bow shock by Scarf *et al.* (1970) and are called ion acoustic waves (Gurnett and Frank, 1978). Ion acoustic waves are very similar to sound waves in an ordinary gas and are driven by ions escaping from the shock. Since these waves are driven by ions, they are confined to the ion foreshock. A wideband spectrogram of ion acoustic waves detected by the Voyager 1 spacecraft upstream of Jupiter's bow shock is shown in Figure P32. As can be seen, the ion acoustic waves have relatively narrow bandwidths and switch on and off abruptly. The abrupt onsets and terminations indicate that the mode is very close to marginal instability. The peak frequencies of the ion acoustic waves (~ 2 kHz) are well below the electron plasma frequency (f_{pe} ~ 5 kHz) but still above the ion plasma frequency (f_{pi} ~ 120 Hz). As can be seen from Table P9, the ion acoustic mode can only propagate at frequencies below the ion plasma frequency. This discrepancy is believed to occur because the waves have very short wavelengths, thereby introducing Doppler shifts due to the motion of the solar wind. For a wave of wavelength λ and frequency f in the plasma rest frame, the frequency f' detected in the spacecraft rest frame is given by

$$f' = f + \frac{V_{sw}}{\lambda} \cos \theta_{kv} \qquad \text{(P15)}$$

where V_{sw} is the solar wind speed and θ_{kv} is the angle between the propagation vector $\vec{k}$ and the solar wind velocity. The shortest wavelength that can exist in a plasma is $\lambda_{min} = 2\pi\lambda_D$, where λ_D is a characteristic length called the Debye length. For the plasma parameters that exist in the solar wind upstream of Jupiter, the shortest wavelength is about $\lambda_{min} \approx 240$ m. The maximum Doppler shift, which is given by the second term on the right-hand side of equation (P11), is then about 1.7 kHz, which is comparable to the highest frequencies observed. Ion acoustic waves have only been reported upstream of the bow shocks at Earth, Mars and Jupiter. For unknown reasons, possibly due to instrumental limitation, ion acoustic waves have not been observed upstream of the bow shocks at Venus, Saturn, Uranus or Neptune.

The bow shock crossings at Venus, Earth, Mars, and all four of the giant planets can be easily identified in the plasma wave data by an intense broadband burst of electric field noise at the shock. This noise was first discovered in the Earth's bow shock by Fredricks *et al.* (1968). A wideband frequency–time spectrogram showing the shock-related electric field noise observed during the Voyager 1 crossing of Jupiter's bow shock is given in Figure P33. This is the same shock crossing shown in Figure P31. Note the electron plasma oscillations at ~ 6 kHz, increasing slowly in frequency as the spacecraft approaches the shock. The electric field noise at the shock extends up to a frequency of about 3 kHz and has a peak broadband intensity of about 1 mV m^{-1}. This noise is believed to be caused by solar wind ions that are magnetically reflected by the shock, thereby forming a gyrating ion beam that excites electrostatic waves via a two-stream instability. Currents flowing along the shock surface may also in some cases contribute to the generation of electrostatic waves. Earlier it was thought that these electrostatic waves played the dominant role in heating the plasma at collisionless shocks (Fredricks *et al.*, 1968). However, more recent studies by Scudder *et al.* (1986) and others suggest that these waves probably act only to thermalize the particle distribution, and that other processes, such as acceleration by quasi-static electric fields and magnetic reflection, are primarily responsible for converting the directed solar wind flow into a heated distribution at the shock.

Trapped continuum radiation

After the shock, the next boundary of interest is the magnetopause. This boundary forms the effective obstacle for the solar wind flow around the planet and is shown by a dashed line in Figure P30. Because the planetary magnetic field provides most of the pressure inside of the magnetosphere, an abrupt drop in the plasma density occurs at the magnetopause, thereby forming a low-density magnetospheric cavity. Since the electron plasma frequency is lower in the magnetosphere than in the solar wind, electromagnetic radiation can be trapped in the magnetospheric cavity. This trapped radiation was first discovered in the Earth's magnetosphere by Gurnett and Shaw (1973) and is called continuum radiation. Since then, trapped continuum radiation has been observed at three of the giant planets, Jupiter, Saturn and Uranus. No trapped continuum radiation was observed at Neptune, probably because the Voyager plasma wave instrument did not have sufficient sensitivity to detect this radiation at Neptune. The trapped continuum radiation at Jupiter is one of the most intense emissions observed at any of the planets. Since no magnetospheric cavity exists at Venus and Mars, trapped continuum radiation cannot occur at either of these planets. For a review of continuum radiation in planetary magnetospheres see Kurth (1991).

An example of trapped continuum radiation is shown in Figure P34. This spectrogram shows the Voyager 1 crossing of the magneto-

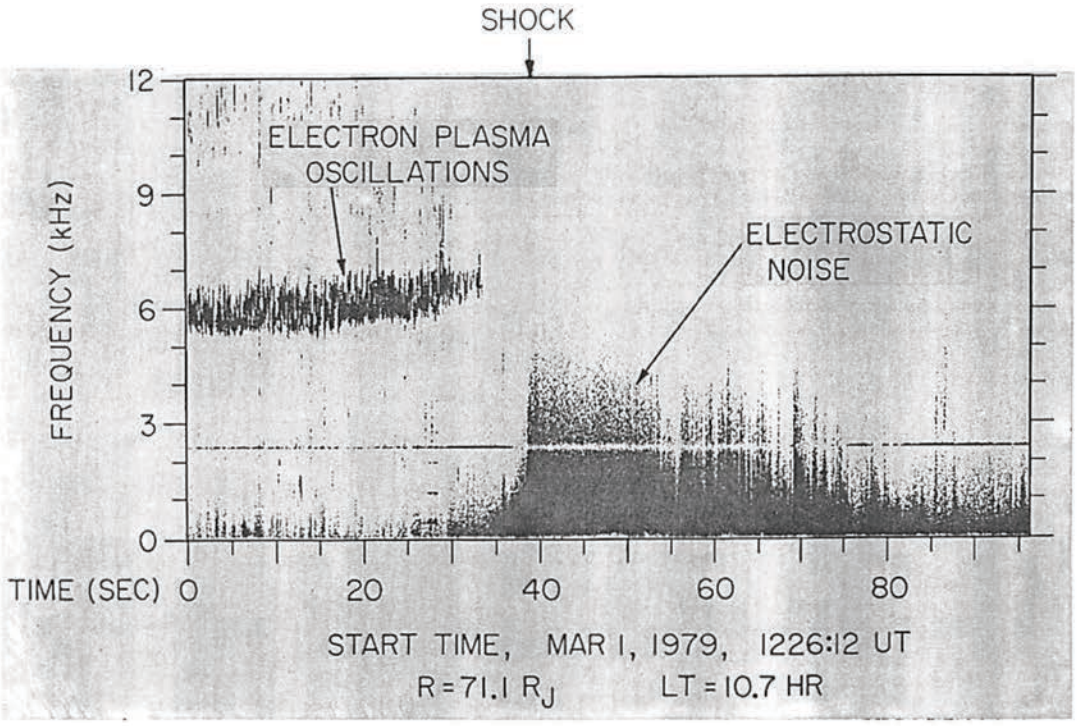

Figure P33 The Voyager 1 inbound crossing of Jupiter's bow shock. An abrupt burst of broadband electric field noise can be seen at the shock. This noise is believed to be caused by ion beams gyrating back into the solar wind from the shock. Electron plasma oscillations can also be seen upstream of the shock.

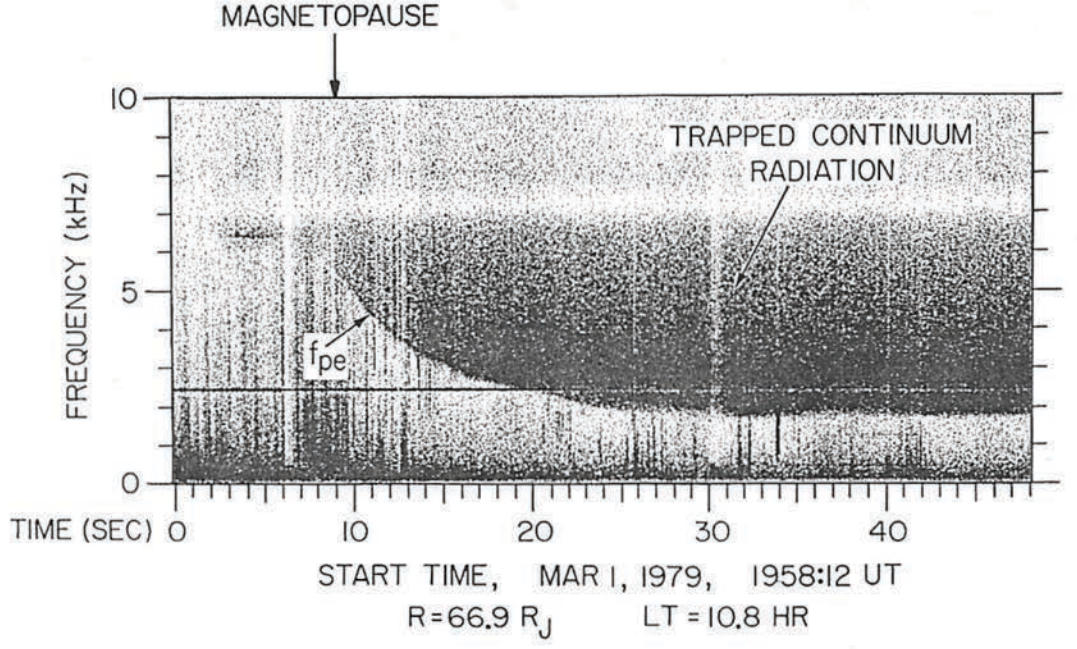

Figure P34 The inbound Voyager 1 crossing of Jupiter's magnetopause. The intense band of noise from about 2 to 7 kHz is continuum radiation trapped in the low-density magnetospheric cavity. The low-frequency cut-off of the continuum radiation is at the electron plasma frequency, f_{pe}.

pause at Jupiter. The continuum radiation consists of the dark band of noise extending upward from about 1 kHz, gradually fading into the receiver background noise above about 7 kHz. The sharp, low-frequency cut-off of the radiation at f_{pe} is believed to be caused by the reflection of free space (L,O) mode electromagnetic waves at the local electron plasma frequency. As can be seen from Table P10, the free space L,O mode can only propagate at frequencies $f > f_{pe}$. Free space (R,X) mode radiation is also most likely present. However, the low-frequency cut-off of the R–X mode is always above f_{pe}, so the L–O mode determines the low-frequency cut-off. The monotonic decrease in the low-frequency cut-off, from about 6.2 to 1.8 kHz over a period of about 20 s, is caused by the rapidly declining plasma

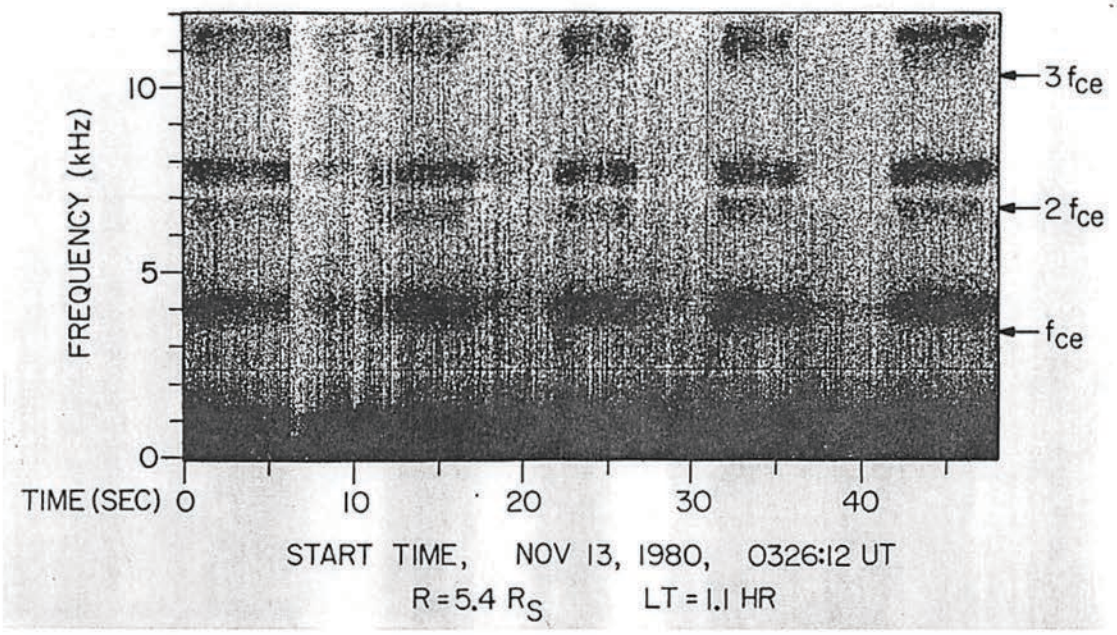

Figure P35 An example of electrostatic electron cyclotron harmonic (ECH) waves in Saturn's magnetosphere. These emissions occur in narrow bands slightly above harmonics of the electron cyclotron frequency, f_{ce}.

density as the spacecraft passes through the magnetopause. Note from equation (P9) that the electron plasma frequency is proportional to the square root of the electron density. The thickness of the magnetopause is controlled mainly by the cyclotron radius of magnetosheath ions as they gyrate into the region of strong field inside the magnetosphere. Continuum radiation comparable to Figure P33 is observed throughout the magnetospheric cavity of Jupiter. Once generated, the radiation is believed to undergo repeated reflections from the walls of the cavity, eventually building up to an equilibrium level throughout the cavity. Small random Doppler shifts caused by repeated reflections from the walls of the magnetospheric cavity, which are continuously in motion, are believed to spread the radiation into a nearly continuous spectrum, hence the term continuum.

Electron cyclotron and upper hybrid waves

For the magnetized planets, the magnetic field within the magnetosphere is generally much stronger than in the solar wind. The electron cyclotron frequency then plays an important role in controlling the types of waves that are generated. In the Earth's magnetosphere it has been known for many years that strong electrostatic emissions are generated near harmonics of the electron cyclotron frequency (Kennel *et al.*, 1970; Shaw and Gurnett, 1975). These emissions are part of a band structure that is often referred to as electron cyclotron waves (Table P10). The free energy source of these waves consists of electrons with a loss cone or ring type of distribution function. Loss-cone velocity distributions are a characteristic feature of planetary radiation belts. Charged particles moving within a well-defined cone of angles around the magnetic field (the loss cone) strike the atmosphere and are lost from the system, thereby producing a hole in the particle velocity distribution.

Electron cyclotron waves are found in the magnetosphere of the Earth and all the giant planets. Typically these waves are most intense near half-integral harmonics $(n + \frac{1}{2})f_{ce}$ of the electron cyclotron frequency. Usually the $(n + \frac{1}{2})f_{ce}$ waves occur in two distinct frequency ranges, the first near low-order half-integral harmonics of the electron cyclotron frequency (i.e. $\frac{3}{2}f_{ce}$, $\frac{5}{2}f_{ce}$, etc.), and the second near the upper hybrid resonance frequency, when $(n + \frac{1}{2})f_e \approx f_{UHR}$. The low-order harmonics are often called electron cyclotron harmonic (ECH) waves, and the emissions near the upper hybrid frequency are called upper hybrid resonance (UHR) waves. The emission frequencies depend in a complicated way on the densities and temperatures of the cold and hot components of the plasma, and are almost never exactly at $(n + \frac{1}{2})f_{ce}$. The half-integral notation, $\frac{3}{2}$, $\frac{5}{2}$, etc., is mainly just a convenient label to identify the emission band.

A spectrogram illustrating examples of low-order ($\frac{3}{2}$,$\frac{5}{2}$ and $\frac{7}{2}$) ECH emissions in the magnetosphere of Saturn is shown in Figure P35. The emission frequencies in this case are slightly above the electron cyclotron harmonics. Considerable fine structure can be seen within the emission bands. Electron cyclotron harmonic emissions of this type are typical of all the ECH observations at the giant planets. Usually, the emissions are strongest in a narrow band slightly above the electron cyclotron harmonics. A spectrogram illustrating an example of UHR emissions in the outer region of Jupiter's magnetosphere is shown in Figure P36. The UHR emissions in this case consist of very sharply defined bands near the lower edge of the trapped continuum radiation. The bands switch on and off as plasma density variations cause the upper hybrid resonance frequency to sweep past half-integral harmonics of the electron cyclotron frequency. Strong emissions occur whenever the condition $(n + \frac{1}{2})f_{ce} \simeq f_{UHR}$ is satisfied. The frequency spacing between the bands is roughly the electron cyclotron frequency.

A striking characteristic of both the ECH and UHR waves is their close confinement to the magnetic equator. Figure P37a shows a multichannel plot of electric field intensities from the Voyager 1 pass through the inner region of the Jovian magnetosphere. The ECH and UHR emissions are identified by circles. Figure P37b shows the magnetic latitude λ_m. The magnetic latitude oscillates up and down due to the rotation of Jupiter's magnetic dipole field, which is tilted at an angle of about 10° with respect to the rotational axis. As can be seen, the ECH and UHR waves occur in sharply localized regions centered almost exactly on the magnetic equator crossings. This narrow confinement to a region only 1 or 2 degrees from the magnetic equator is a characteristic feature of all the ECH and UHR observations at the giant planets. A similar effect also occurs in the Earth's magnetosphere, although not as dramatically as at the giant planets.

The reason that the ECH and UHR waves are confined to a narrow region near the magnetic equator is still a subject of investigation. Based on terrestrial studies it is believed that two factors are responsible. First, it is known that the electrons responsible for generating the waves have pitch angles near 90°. Due to the laws governing the motion of trapped radiation belt particles (conservation of the first and second adiabatic invariants), particles with pitch angles near 90° are closely confined to the vicinity of the magnetic equatorial plane. Since this type of highly anisotropic velocity distribution (with pitch angles near 90°) is required to generate the ECH and UHR waves, large wave growth can only occur near the magnetic equator. Second, ray tracing studies show

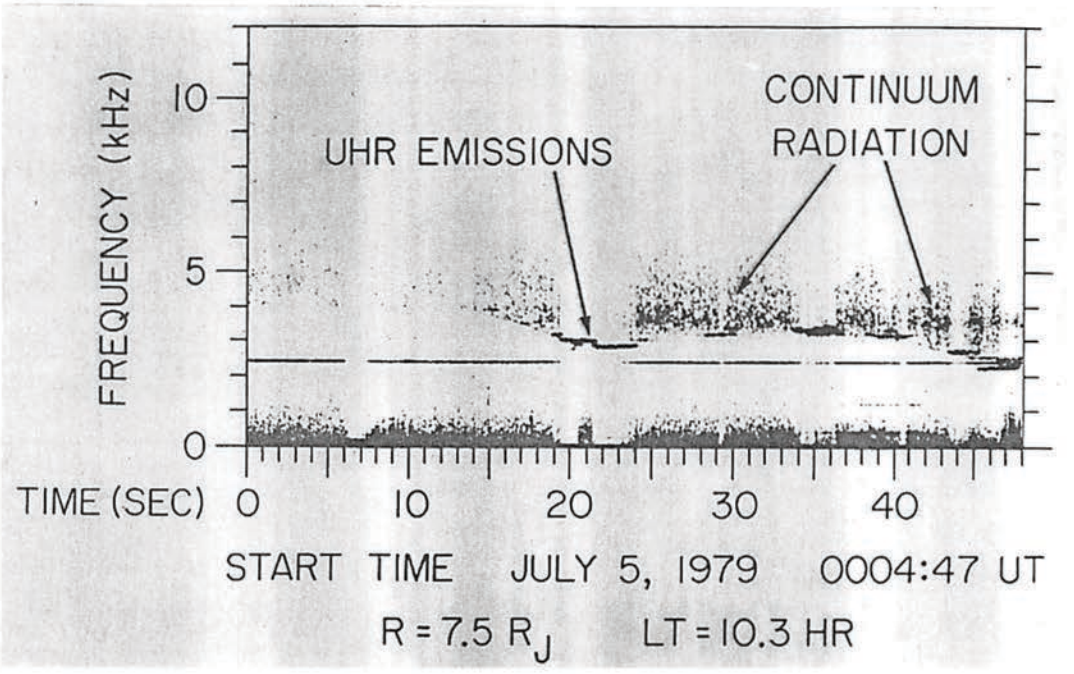

Figure P36 An example of upper hybrid resonance (UHR) emissions in Jupiter's magnetosphere. These emissions occur in narrow bands near the upper hybrid resonance frequency, f_{UHR}.

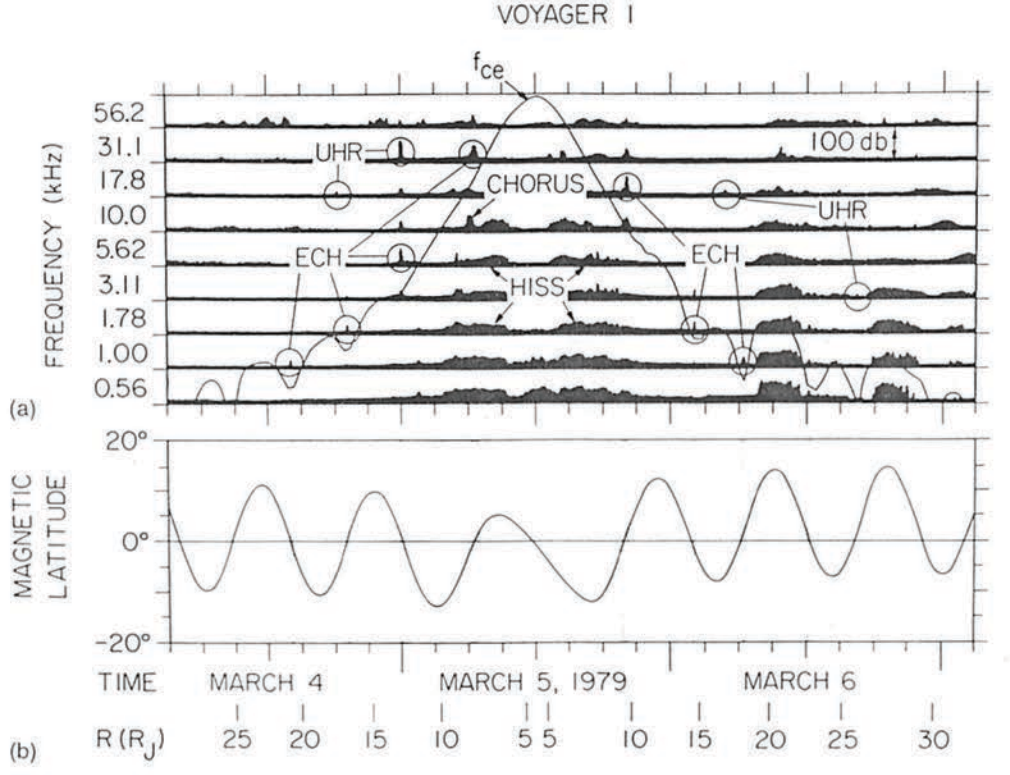

Figure P37 (a) Electric field intensities observed during the Voyager 1 pass through the inner region of the Jovian magnetosphere and (b) the magnetic latitude. Both ECH and UHR waves always occur very close to the magnetic equator.

that the electron cyclotron waves tend to be guided along the magnetic equator. This guiding effect is believed to confine the wave growth to a narrow region along the magnetic equatorial plane.

One may ask what role these electrostatic waves play in the magnetospheres of the giant planets. In the terrestrial magnetosphere, for many years it has been thought that electron cyclotron waves control the loss of trapped radiation belt electrons by scattering particles into the loss cone (Kennel *et al.*, 1970). It seems likely that similar processes are operative at the giant planets. Unfortunately, adequate measurements are not available from the Voyager plasma data in the proper electron energy range (a few hundred eV to several tens of keV) to evaluate this loss mechanism. In the Earth's magnetosphere, UHR emissions are also believed to be a source of free-space electromagnetic radiation. The generation mechanism is believed to involve a mode conversion process by which UHR waves are converted to escaping electromagnetic (L, O mode) radiation. The mode conversion process can be either linear (Jones, 1980) or nonlinear (Melrose, 1981). Trapped continuum radiation is thought to be produced by this mode conversion process (Kurth, 1991).

Whistler-mode emissions

Whistlers are one of the oldest and best-known terrestrial plasma wave phenomena. Whistlers were first observed by ground-based radio receivers (Barkhausen, 1919). The modern theory of whistlers was first proposed by Storey (1953). According to Storey's theory, low-frequency electromagnetic radiation from a lightning discharge is guided along the magnetic field lines through the magnetospheric plasma. Because of the peculiar nature of electromagnetic wave propagation at frequencies below the electron cyclotron frequency, the higher frequencies propagate faster than the lower frequencies. Thus, the broadband impulsive signal produced by a lightning flash is converted into a whistling tone, hence the term 'whistler'. The plasma wave mode involved in the propagation of whistlers is called the whistler mode. Whistler-mode waves are right-hand polarized and propagate at frequencies below either f_{ce} or f_{pe}, whichever is smaller (see Table P10). The whistler mode is highly anisotropic and has a number of unusual characteristics, one of which is that the index of refraction goes to infinity along a cone of directions called the resonance cone (Stix, 1962). This highly anisotropic characteristic accounts for the fact that the wave energy is guided approximately along the magnetic field (see Whistler).

In addition to lightning-generated whistlers, whistler-mode waves can also be spontaneously generated in a magnetized plasmas. These waves are called whistler-mode emissions. Whistler-mode emissions are a common feature of the terrestrial magnetosphere and occur in the magnetospheres of all the giant planets. These emissions are mainly generated in the inner regions of the magnetosphere where the loss cone in the trapped energetic electron distribution provides an effective free energy source. From very general principles (Brice, 1964), it can be shown that the growth of whistler-mode waves leads to a decrease in the pitch angle of resonant electrons, thereby driving the particles toward the loss cone. The growth of whistler-mode waves is widely believed to be the dominant mechanism responsible for the loss of energetic electrons from planetary radiation belts. In a classic paper Kennel and Petschek (1966) showed that the growth of whistler-mode waves puts an upper limit on the energetic electron intensities that can exist in planetary radiation belts.

A representative spectrum of whistler-mode emissions in the inner region of Jupiter's magnetosphere is shown in Figure P38a. This spectrum was obtained in the Io plasma torus, which is a dense torus of plasma produced by gases escaping from Jupiter's moon Io (see Planetary Torus). The plasma in the Io torus is extremely energetic and produces very intense whistler-mode emissions, among the most intense ever observed in a planetary magnetosphere. Two types of emissions are observed, called 'hiss' and 'chorus'. The hiss is an essentially structureless emission. When the hiss signals are played through an audio speaker, they make a steady hissing sound, hence the term 'hiss.' According to current ideas, whistler-mode hiss is believed to represent a fully developed turbulent spectrum in which the wave growth and loss has achieved a steady state equilibrium. In contrast to the whistler-mode hiss, chorus emissions are highly structured. A wideband frequency–time spectrogram of chorus is shown in Figure P39. The term 'chorus' is an old term (Allcock, 1957), and has its origins in the term 'dawn chorus' which refers to the sounds made by a roosting flock of birds at daybreak. The reasons for the complex spectral structure, usually consisting of many discrete

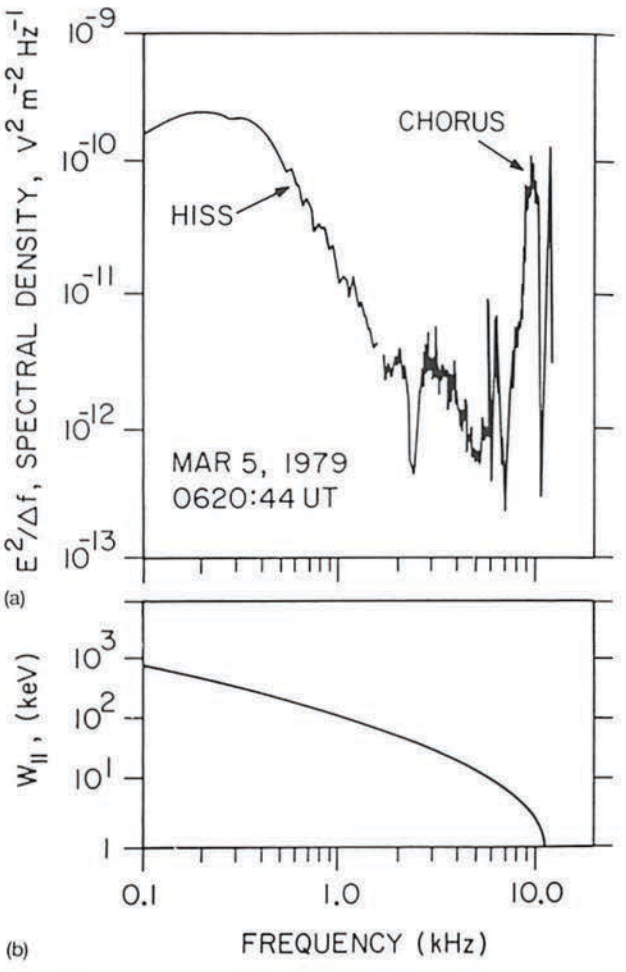

Figure P38 (a) An electric field spectrum of whistler-mode hiss and chorus emissions in Jupiter's Io torus. (b) The energy $W_{\parallel}$ of electrons that are in cyclotron resonance with these waves. The hiss tends to interact with very energetic electrons (~ 100 to 1000 keV), whereas the chorus interacts with much lower energies (~ 1 to 10 keV).

narrowband tones rising in frequency, is poorly understood. The current view is that the waves grow to such large amplitudes that local nonlinear processes play a dominant role in controlling the evolution of the wave. Computer simulations show that particles trapped in the wave field produce isolated wave packets, each of which evolves somewhat differently in time and space.

It is instructive to comment on the electron energies involved in the generation of hiss and chorus. Whistler-mode wave growth proceeds via a resonant process in which a constant force is experienced by a particle undergoing cyclotron motion along a magnetic field line, thereby leading to a deceleration (or acceleration) of the particle and a growth (or damping) of the wave. This process is called cyclotron resonance. The general condition for cyclotron resonance is

$$v_{\parallel Res} = \frac{\omega - n\,\omega_{ce}}{k_{\parallel}} \qquad \text{(P16)}$$

where $v_{\parallel Res}$ is the parallel resonance velocity (the symbol $\parallel$ refers to the component parallel to the magnetic field), ω is the wave frequency, $k_{\parallel}$ is the parallel component of the wave vector and n is an integer. For whistler-mode waves, the $n = 1$ term is usually most important. This resonance is called the first-order cyclotron resonance and occurs when both the wave and the particles (electrons) are rotating in the right-hand sense with respect to the magnetic field. From the propagation characteristics of the wave, $\omega(k)$, one can calculate the parallel energy $W_{\parallel}$ of the resonant electrons. The parallel resonance energy for whistler-mode emissions at Jupiter is

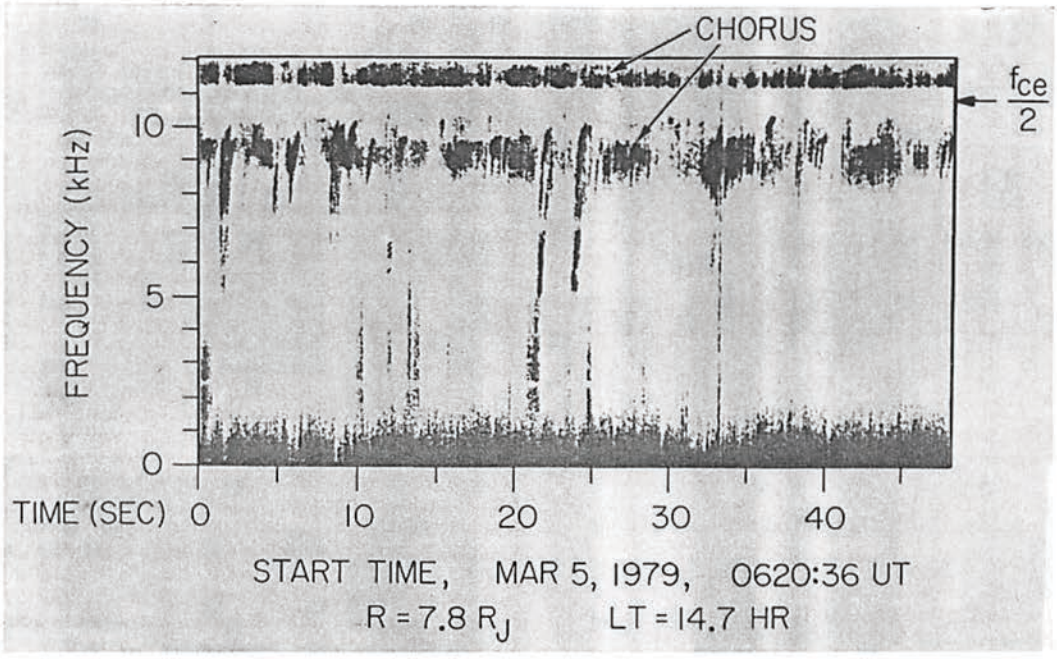

A-693-27

Figure P39 A high-resolution frequency–time spectrogram of chorus emissions. These emissions are highly structured and often consist of narrowband tones rising in frequency with increasing time. Chorus often has a sharp notch in the spectrum at one-half of the electron cyclotron frequency, $f_{ce}/2$.

shown in Figure P38b. As can be seen, the resonance energy decreases rapidly with increasing frequency. The energy of the electrons interacting with the hiss tends to be very high, 100 to 1000 keV, whereas the energy of the electrons interacting with the chorus tends to be much lower, 1–10 keV. This trend, for hiss to resonate with high energies and chorus to resonate with low energies, is typical of whistler-mode emissions at all of the giant planets.

In addition to Earth, three of the giant planets, Jupiter, Saturn and Uranus, have intense whistler-mode hiss and chorus emissions. These emissions occur in the inner regions of the magnetosphere where the trapped radiation belt electron intensities are the highest. The existence of whistler-mode emissions at Neptune is unclear. Some very weak emissions were observed in the spectrum analyzer data that are probably whistler-mode hiss. However, no chorus was observed in any of the wideband data. The absence of chorus at Neptune could be due to the low radiation belt intensities, which were the lowest of any of the giant planets. It can be shown that the growth rate of whistler-mode emissions increases in direct proportion to the intensity of the resonant electron. The extremely low whistler-mode emission intensities at Neptune could therefore be due to the low radiation belt electron intensities. On the other hand, the spacecraft did not pass through the equatorial region of the radiation belt where the highest wave amplitudes would be expected. Thus, it may be that strong whistler-mode emissions were present in the magnetosphere of Neptune, but the spacecraft did not pass through the proper region to observe these waves.

A third type of whistler-mode emission also occurs in planetary magnetospheres. This emission occurs in the auroral regions and is called auroral hiss. Auroral hiss is a nearly structureless emission and is believed to propagate at wave normal angles near the resonance cone. Near the resonance cone the whistler mode is very nearly electrostatic, with small magnetic fields, short wavelengths and low propagation speeds. These short-wavelength, quasi-electrostatic, whistler-mode waves are sometimes called lower hybrid waves, since they become completely electrostatic at the lower-hybrid resonance frequency, f_{LHR}. Because of the low propagation velocity, auroral hiss can be excited by beams, very similar to electron plasma oscillations. Auroral hiss has been extensively studied in the Earth's magnetosphere, where it has been shown that the emissions are produced by the same electron beams that produce the auroral light emission, hence the term 'auroral hiss.' Auroral hiss has also been observed at Jupiter by Voyager 1 (Gurnett *et al.*, 1979) and by Ulysses (Stone *et al.*, 1992). In both cases the identification was based on the similarity to terrestrial auroral hiss and not on a direct correlation with the aurora on Jupiter. No auroral hiss was observed at Saturn, Uranus or Neptune, most likely because the spacecraft did not pass through the proper region to observe such emissions.

Electrostatic ion cyclotron waves

Electrostatic ion cyclotron waves occur in discrete bands between harmonics of the ion cyclotron frequency (Table P10), very similar to electron cyclotron waves, which occur between harmonics of the electron cyclotron frequency. One of the unique features of the electrostatic ion cyclotron mode is that it is driven unstable by relatively weak field line currents. This feature led Kindel and Kennel (1971) to predict that electrostatic ion cyclotron waves would be produced by field-aligned currents over the Earth's auroral regions. The existence of such waves was subsequently confirmed by Kintner, Kelley and Mozer, (1978), using data from the polar orbiting S3-3 satellite. A representative spectrum of electrostatic ion cyclotron waves observed along the Earth's auroral field lines is show in Figure P40. Strong enhancements can be seen just above the lowest three harmonics of the proton (H^+) cyclotron frequency. Originally it was thought that these waves were driven by field-aligned currents. However, more recent studies suggest that these waves are produced by ion beams accelerated upward along the auroral field lines by the same quasi-static electric fields that produce the electron precipitation responsible for the aurora. Electrostatic ion cyclotron waves are also sometimes observed near the magnetic equatorial plane. These waves are believed to be driven by energetic ions trapped near the magnetic equator.

Observations of electrostatic ion cyclotron waves in other planetary magnetospheres are very limited. Since the Voyager spacecraft did not pass through the high-latitude auroral regions at the giant planets, with the possible exception of Neptune, no opportunity existed to search for electrostatic ion cyclotron waves driven by auroral processes. Barbosa and Kurth (1990) have interpreted a narrow band of low-frequency waves observed in the cold plasma torus at Jupiter as electrostatic ion cyclotron waves. They suggest that these waves are produced by a charge-exchange interaction between neutral gas emissions from volcanoes on Io and the rapidly rotating Io plasma torus, which is locked to the rotation of Jupiter. This charge-exchange process produces a ring-type ion distribution (sometimes called pick-up ions) and is expected to provide a very effective free energy source for generating electrostatic ion cyclotron waves. Barbosa and Kurth (1990) have also interpreted a band of low-

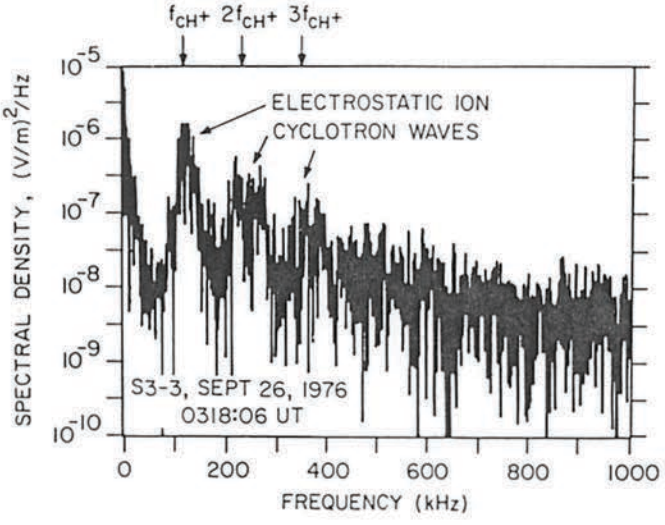

Figure P40 An electric field spectrum of electrostatic ion cyclotron waves observed in the Earth's magnetosphere by the S3–3 spacecraft. These waves occur between harmonics of the proton cyclotron frequency (f_{CH^+}) and are driven by currents flowing along the auroral field lines. (Kintner, Kelley and Mozer, 1978; copyright American Geophysical Union.)

frequency electric field noise in Neptune's magnetosphere as electrostatic ion cyclotron waves, also driven by the same charge-exchange process. Unfortunately, in neither case is it possible to confirm the electrostatic character of the waves, so the identification of the mode is not completely certain.

Electromagnetic ion cyclotron waves

Electromagnetic ion cyclotron waves are very similar to whistler-mode waves, except that they are left-hand polarized and propagate below the ion cyclotron frequency (Table P10). Since the ion cyclotron frequency is much lower than the electron cyclotron frequency [equation (P10)], ion cyclotron waves necessarily occur at extremely low frequencies, typically a few hundred hertz or less. Since the wave field of an electromagnetic ion cyclotron wave rotates in the same sense as positive ions (i.e. left-hand with respect to the magnetic field), these waves interact strongly with positively charged ions. Almost all of the ions observed in planetary magnetospheres are positively charged. The cyclotron resonance condition is identical to equation (P16), except that (e) is replaced by (i). Electromagnetic ion cyclotron waves are driven unstable by a loss cone in the energetic ion distribution. Since a loss cone is always present in a planetary radiation belt, the growth of these waves provides a mechanism for scattering energetic ions into the loss cone, thereby controlling the loss of radiation belt ions.

Despite the intense theoretical interest in the generation of electromagnetic ion cyclotron waves in planetary magnetospheres, relatively few observations are available. The first report of spontaneously generated electromagnetic ion cyclotron waves in the Earth's magnetosphere was by Taylor, Parady and Cahill (1975). These and other subsequent observations (Kintner, Kelley and Mozer, 1977; Roux *et al.*, 1982) have shown that electromagnetic ion cyclotron waves are generated in the Earth's radiation belt during magnetic storms, when intense fluxes of energetic (10 to 100 keV) ions are injected deep into the inner regions of the magnetosphere. Electromagnetic ion cyclotron waves have also been observed at Jupiter by Thorne and Scarf (1984) using Voyager 1 measurements, and by Stone *et al.* (1992) using Ulysses measurements. In both cases intense waves were observed at frequencies below the proton cyclotron frequency. The Ulysses observations are particularly important because the magnetic field of the wave was measured, which confirms that the waves are electromagnetic and not electrostatic (Voyager had only an electric antenna). The ion precipitation produced by these waves is believed to be responsible for the extreme ultraviolet (EUV) aurora at Jupiter (Thorne and Moses, 1983). Using Voyager 2 Neptune data, Gurnett *et al.* (1989) reported observations of a strong band of electric field noise at Neptune at frequencies below the proton cyclotron frequency. This band of electric field noise was tentatively identified as electromagnetic ion cyclotron waves. However, since no wave magnetic field measurements were available, it was not possible to establish definitely the mode of propagation.

Conclusion

This review has described the primary types of plasma waves observed in the vicinity of the planets Venus, Mars, Earth, Jupiter, Saturn, Uranus and Neptune. These observations are summarized in Table P11. By necessity we have not attempted to describe the detailed nature of the observations at each planet. For a more detailed description, see the review by Kurth and Gurnett (1991). In making comparisons between these planets it must be recognized that the observations are in many cases incomplete, particularly at Uranus and Neptune, where the available data are limited to only one pass by the planet. At the giant planets almost no information is available at high magnetic latitudes, a region that we know from terrestrial observations has many complex aurora-related plasma wave emissions. No plasma wave observations have been obained at Mercury and Pluto. Thus there are very significant gaps in our knowledge. It is likely to be many years before these gaps are filled. The most promising missions for future plasma wave investigations are Galileo, which is to orbit Jupiter in late 1995, and Cassini, which is to orbit Saturn early in the 21st century; both spacecraft include plasma wave instruments.

Donald A. Gurnett

Bibliography

Allcock, G. McK. (1957) A study of the audio-frequency radio phenomena known as 'dawn chorus,' *Aust. J. Phys.*, **10**, 286–98.

Barbosa, D.D., and Kurth, W.S. (1990) Theory and observations of electrostatic ion waves in the cold ion torus. *J. Geophys. Res.*, **95**, 6443–50.

Table P11 A summary of the observations of various types of plasma waves at all the planets except Merccury and Pluto

Type of plasma wave	Venus	Earth	Mars	Jupiter	Saturn	Uranus	Neptune
Upstream electron plasma oscillations	×	×	×	×	×	×	×
Upstream ion acoustic waves		×	×	×			
Electrostatic noise at the bow shock	×	×	×	×	×	×	×
Electron cyclotron harmonic waves		×		×	×	×	×
Upper hybrid resonance waves		×		×	×	×	×
Whistler-mode hiss		×		×	×	×	×(?)
Whistler-mode chorus		×		×	×	×	
Whistler-mode auroral hiss		×		×			
Electrostatic ion cyclotron waves		×		×(?)			×(?)
Ion cyclotron whistlers (lightning)		×					
Electromagnetic ion cyclotron emissions		×		×			×(?)

Barkhausen, H. (1919) Zwei mit Hilfe der neuen Verstärker entdeckte Erscheinungen. *Phys. Z.*, **20**, 401.
Barrington, R.E. and Belrose, J.S. (1963) Preliminary results from the very-low frequency receiver aboard Canada's Alouette satellite. *Nature*, **198**, 651–6.
Brice, N. (1964) Fundamentals of very low frequency emission generation mechanisms. *J. Geophys. Res.*, **69**, 4515–22.
Fahleson, U.V. (1967) Theory of electric field measurements conducted in the magnetosphere with electric probes. *Space Sci. Rev.*, **7**, 238–62.
Fredricks, R.W., Kennel, C.F., Scarf, F.L. *et al.* (1968) Detection of electric-field turbulence in the Earth's bow shock. *Phys. Rev. Lett.*, **21**, 1761–4.
Grard, R., Nairn, C., Pedersen, A. *et al.* (1991) Plasma and waves around Mars. *Planet. Space Sci.*, **39**, 89–98.
Gurnett, D.A. (1992) Planetary radio emissions, in *Astronomy and Astrophysics Encyclopedia* (ed. S.P. Maran). New York: Van Nostrand Reinhold, p. 535–7.
Gurnett, D.A. and Frank, L.A. (1978) Ion acoustic waves in the solar wind. *J. Geophys. Res.*, **83**, 58–74.
Gurnett, D.A., Kurth, W.S., Poynter, R.L. *et al.* (1989) First plasma wave observations at Neptune. *Science*, **246**, 1494–8.
Gurnett, D.A., Kurth, W.S., Roux, A. *et al.* (1991) Lightning and plasma wave observations from the Galileo flyby of Venus. *Science*, **253**, 1522–5.
Gurnett, D.A., Kurth, W.S. and Scarf, F.L. (1979a) Plasma wave observations near Jupiter: initial results from Voyager 2. *Science*, **206**, 987–91.
Gurnett, D.A., Kurth, W.S. and Scarf, F.L. (1979b) Auroral hiss observed near the Io plasma torus. *Nature*, **280**, 767–70.
Gurnett, D.A., Kurth, W.S. and Scarf, F.L. (1981) Plasma waves near Saturn: initial results from Voyager 1. *Science*, **212**, 235–9.
Gurnett, D.A., Kurth, W.S., Scarf, F.L. and Poynter, R.L. (1986) First plasma wave observations at Uranus. *Science*, **233**, 106–9.
Gurnett, D.A. and O'Brien, B.J. (1964) High-latitude geophysical studies with satellite Injun 3, 5. Very-low-frequency electromagnetic radiation. *J. Geophys. Res.*, **69**, 65–89.
Gurnett, D.A., and Shaw, R.R. (1973) Electromagnetic radiation trapped in the magnetosphere above the plasma frequency. *J. Geophys. Res.*, **78**, 8136–49.
Gurnett, D.A., Shaw, R.R., Anderson, R.R. *et al.* (1979) Whistlers observed by Voyager 1: Detection of lightning on Jupiter. *Geophys. Res. Lett.*, **6**, 511.
Jones, D. (1980) Latitudinal beaming of planetary radio emissions. *Nature*, **288**, 225–9.
Kennel, C.F., and Petschek, H.E. (1966) Limit on stably trapped particle fluxes. *J. Geophys. Res.*, **71**, 1–28.
Kennel, C.F., Scarf, F.L., Fredricks, R.W. *et al.* (1970) VLF electric field observations in the magnetosphere. *J. Geophys. Res.*, **75**, 6136–52.
Kindel, J.M. and Kennel, C.F. (1971) Topside current instabilities. *J. Geophys. Res.*, **76**, 3055–78.
Kintner, P.M., and Gurnett, D.A. (1977) Observations of ion cyclotron waves within the plasmasphere by Hawkeye 1. *J. Geophys. Res.*, **82**, 2314–8.
Kintner, P.M., Kelley, M.C. and Mozer, F.S. (1978) Electrostatic hydrogen cyclotron waves near one Earth radius altitude in the polar magnetosphere. *Geophys. Res. Lett.*, **5**, 139–42.
Krall, N.A., and Trivelpiece, A.W. (1973) *Principles of Plasma Physics*. New York: McGraw-Hill.
Kurth, W.S. (1991) Continuum radiation in planetary magnetospheres, in *Planetary Radio Emissions III* (eds H.O. Rucker, S.J. Bauer and M.L. Kaiser). Vienna, Austria. Verlage der Osterreichischen Akademie der Wissenschaften, p. 329–50.
Kurth, W.S., and Gurnett, D.A. (1991) Plasma waves in planetary magnetospheres. *J. Geophys. Res.*, **96**, 18877–991.
Melrose, D.B. (1981) A theory for the nonthermal radio continuum in the terrestrial and Jovian magnetospheres. *J. Geophys. Res.*, **86**, 30–6.
Roux, A., Perraut, S. Rauch, J.L. *et al.* (1982) Wave–particle interactions near ω_{He^+} observed on board Geos 1 and 2, 2. Generation of ion cyclotron waves and heating of He^+ ions. *J. Geophys. Res.* **87**, 8174–90.
Scarf, F.L., Gurnett, D.A. and Kurth, W.S. (1979) Jupiter plasma wave observations: an initial Voyager 1 overview. *Science*, **204**, 991–5.
Scarf, F.L., Taylor, W.W.L. and Green, I.M. (1979) Plasma waves near Venus: initial observations. *Science*, **203**, 748–50.
Scarf, F.L., Fredricks, R.W., Frank, L.A. and Neugebauer, M. (1971) Nonthermal electrons and high-frequency waves in the upstream solar wind, 1. Observations. *J. Geophys. Res.*, **76**, 5162–71.
Scarf, F.L., Gurnett, D.A., Kurth, W.S. and Poynter, R.L. (1982) Voyager 2 plasma wave observations at Saturn. *Science*, **215**, 587–94.
Scarf, F.L., Fredricks, R.W., Frank, L.A. *et al.* (1970) Direct correlations of large amplitude waves with suprathermal protons in the upstream solar wind. *J. Geophys. Res.*, **75**, 7316–72.
Scudder, J.D., Mangeney, A., Lacome, C. *et al.* (1986) The resolved layer of a collisionless, high β, supercritical, quasi-perpendicular shock wave, 3. Vlasov electrodynamics. *J. Geophys. Res.*, **91**, 11075–97.
Shaw, R.R. and Gurnett, D.A. (1975) Electrostatic noise bands associated with the electron gyrofrequency and plasma frequency in the outer magnetosphere. *J. Geophys. Res.*, **80**, 4259–71.
Stix, T. (1962) *The Theory of Plasma Waves*. New York: McGraw-Hill, 110 pp.
Stone, R.G., Pedersen, B.M., Harvey, C.C. *et al.* (1992) Ulysses radio and plasma wave observations in the Jupiter environment. *Science*, **257**, 1524–30.
Storey, L.R.O. (1953) An investigation of whistling atmospherics. *Phil. Trans. Roy. Soc. London*, **A, 46**, 113–41.
Taylor, W.W.L., Parady, B.K. and Cahill, L.J. Jr, (1975) Explorer 45 observations of 1- to 30-Hz magnetic fields during magnetic storms. *J. Geophys. Res.*, **80**, 1271–86.
Thorne, R.M. and Moses, J. (1983) Electromagnetic ion-cyclotron instability in the multi-ion Jovian magnetosphere. *Geophys. Res. Lett.*, **10**, 631–4.
Thorne, R.M., and Scarf, F.L. (1984) Voyager 1 evidence for ion-cyclotron instability in the vicinity of the Io plasma torus, *Geophys. Res. Lett.*, **11**, 263–6.

Acknowledgement

This research was supported by NASA through contract 959193 with the Jet Propulsion Laboratory.

Cross references

Heliosphere
Magnetospheres of the outer planets
Planetary torus
Shock waves
Solar wind
Thermal plasma instrumentation
Voyager missions
Whistler

PLATE TECTONICS

The Earth's solid surface behaves in most places as if it were divided into a number of almost rigid 'plates'. Any horizontal motion of a rigid plate on a spherical Earth is necessarily a rotation about an axis through the center. This axis cuts the surface at the 'pole of rotation'. The plates move relative to one another over the asthenosphere (q.v.) at speeds of the order of 10–100 mm per year. Two good modern textbooks on the subject are Cox and Hart (1986) and Fowler (1990).

Figure P41 is a map of shallow earthquakes, which mark the plate boundaries well in the oceans but less so in continental areas. At mid-ocean ridges (Figure P42) the ocean is typically 2.5 km shallower than average; the plates are moving apart; hot, soft asthenosphere rises and turns into hard, cold sea floor; and there are only shallow earthquakes. The opposite sides of oceanic plates usually have 'subduction zones' where the plates bend and go down into the mantle. These zones are marked by trenches several kilometers deeper than normal ocean nearby; by earthquakes which are shallow near the trenches, and become deeper with distance away from them; and by lines of andesitic volcanoes above the earthquakes 100–200 km deep.